Bar-Ilan University

The Metallic State in Periodic Granular Systems

Avital Fried

Submitted in partial fulfillment of the requirement for the Master's Degree in the Department of Physics,

Bar-Ilan University

Ramat-Gan, Israel 2019

This work was carried out under the supervision of Prof. Aviad Frydman of the Department of Physics, Bar-Ilan University.

Acknowledgements

I would like to express my deep and sincere gratitude to my research supervisor, Prof. Aviad Frydman for giving me the opportunity to do research and providing invaluable guidance throughout this research. I couldn't have done this work without his guidance. He helped me a lot during the research and the writing of this thesis and made sure that I'm more than ready for the thesis defense, and for that I'm grateful.

In addition, I would like to thank Prof. Beena Kalisky for measuring my samples. Beena and her student Andres worked hard in order to provide a satisfying information about the superconductivity of the dots and helped a lot in our work.

My sincere thanks also go to Dr. Michael Stern and his student Tikai Chang, which evaporated Nb for me and helped in making the samples as good as possible.

Another thank is to Tal Havdala, for doing evaporations for me and for always be there for consulting the right way for preparing samples and giving good advises.

I also want to thank Moshe Feldberg and Tali Shaharabani, for evaporating Au for my samples and investing time and effort trying to help and find the perfect way to fulfil my requests.

Last but not least, I would like to thank my colleague friends and my Cooper pair over the sea, for supporting me in hard times during this challenging period. I couldn't have done it without you. It means a lot to me:)

Contents

Abstract

The study of 2 dimensional (2D) systems was initiated several decades ago. Since the scaling theory of localization, it has been accepted that a metallic state cannot exist in 2D systems, in the absence of strong interactions. Nevertheless, an anomalous metallic regime has been reported recently in variety of 2D superconducting films. In this work, we investigate the phenomenon of 2D "metallic phase" and characterize it. We focus our research on periodic granular systems, in which strong signs of the metallic state were observed in the past. Moreover, in these kind of systems the transition between an insulator to superconductor is governed mainly by the coupling energy between the grains.

In order to characterize the metallic state, we study how it is influenced by a physical barrier between the superconducting grains. For that purpose, we fabricated two types of samples: one contains an oxide layer between the superconducting dots, and the other sample has a clean interface. Transport measurements were performed on the samples at low temperatures, while thin metallic layers were evaporated on top of the dots. The metallic layers enhance the coupling between the dots and influence the system's state.

The main result of our work is that the sample with clean interface showed a direct transition between an insulator to a superconductor, while the sample with the barrier showed a resistance saturation, which implies a metallic behavior.

Our conclusion is that the metallic state appears in 2D systems when the transmission between the superconducting dots and the coupling metal is low. This is caused either by a physical barrier or by a mismatch of the fermi velocities of the superconducting and the metallic materials.

1. Theoretical background

1.1. Quantum phase transition

A classical phase transition is governed by thermal fluctuations and is characterized by a critical temperature, above which the system is in one phase, and below it – the system transits to another phase. An example for a phase transition is superconductivity in which the system transits from a normal state to a superconducting state at a critical temperature, T_c. In recent years there has been a lot of interest in a different type of phase transition, a quantum-phase transition[1] (QPT). Unlike thermal phase transitions that are governed by thermal fluctuations, a QPT is controlled by quantum fluctuations at T=0 as a function of a tuning parameter, g, which is non-thermal. At T=0, the phase transition occurs at a quantum critical point (QCP), $g=g_c$, while at T>0, a quantum critical region (QCR) is generated around g_c, as sketched in Fig. 1.1.

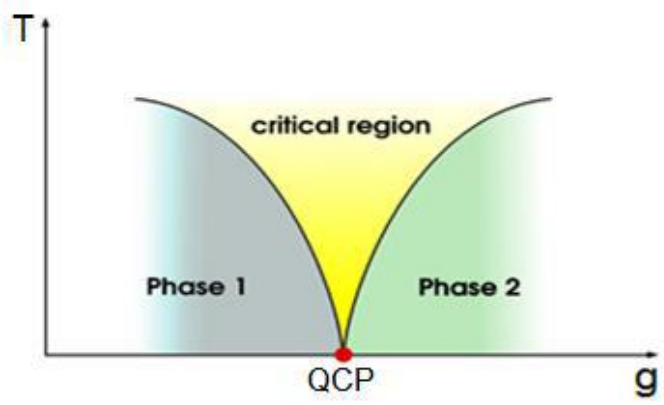

Figure. 1.1: An illustration of a quantum phase transition as a function of a tuning parameter g, where g_c is the critical point T=0. At T>0, there is a quantum critical region with a temperature dependent width**.**

In this QCR, the system doesn't belong totally to either one of the system's states and is characterized by quantum fluctuations. Quantum fluctuations have an energy scale of $\hbar\omega$, while classical fluctuations have an energy scale of K_BT. In the QCR $\hbar\omega > K_BT$, so the quantum fluctuations are the ones which dominate the system's behavior. An

example for a QPT is the superconductor insulator transition, which will be the main focus of this work.

1.2. SIT – Superconductor Insulator Transition

The phenomenon of superconductivity is well understood in a perfect crystal (i.e. in the absence of impurities) thanks to the work of Bardeen, Schrieffer, and Cooper (BCS)[2]. They established the most common theory of superconductivity by identifying the mechanism of effective attraction between electrons, mediated by the electron-phonon coupling. Due to this attraction, the electrons form Cooper pairs that condensate into macroscopic superconducting state. Following BCS, Anderson[3] predicted that the superconducting phase can exist even in the presence of (nonmagnetic) impurities. This was found to be true in weak disorder. However, experiments showed that for strong enough disorder the system transits into an insulator state[4-7], in what has been named the superconductor insulator transition (SIT). Thin films became a matter of great interest in the context of the possibility to observe this transition[8-11]. Experimentally a wide variety of tuning parameters, g, was used: thickness, magnetic field, disorder level, chemical structure, etc. [5, 7, 8, 12-19]. An example for an SIT that is tuned by disorder can be seen in Fig. 1.2 that presents transport measurements in a sample of an amorphous indium oxide (InO) film driven continuously through a disorder-induced SIT. Changing the disorder level is achieved by low-temperature thermal annealing.

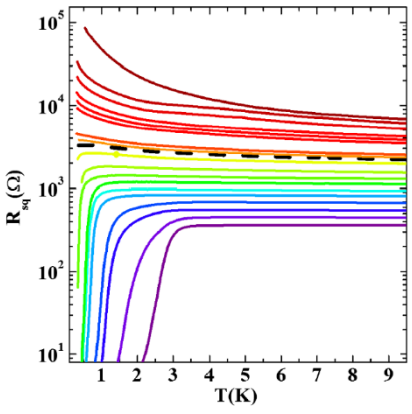

Figure. 1.2: R□ versus T of an InO film for different annealing stages. The quantum phase transition is manifested as the gradual change of the ground state from insulator to superconductor as R□ is lowered. The dashed line curve separates the insulating and superconducting stages. Taken from[11].

The research of the SIT focuses on the physics of films in the quantum critical regime, since in this regime the behavior of the films is special and number of non-trivial effects are observed, such as a unique I-V curves[20].

There are several theories that have been proposed in order to explain the SIT. In this work, we will focus on the "bosonic model", as it is the theory which is the most relevant to our experimental system, i.e. a granular system.

1.3. The bosonic model

The superconducting wave function is expressed by: $\psi = \psi_0 e^{i\theta}$, where ψ_0 represents the amplitude and θ represents the phase of the condensate. The amplitude depends on the density of Cooper pairs, n, while the phase depends on the coupling between all parts of the system. Disorder can influence both these parameters and therefore, the superconductivity can be suppressed either by phase or by amplitude fluctuations. The bosonic model is based on phase fluctuations being the dominant ones. Hence, the creation of a global superconductivity in this model is achieved by attaining a global phase coherence.

In superconductors of low dimensionality, fluctuations in the phase of the wave function state are enhanced, and different part of the system have different phases. A granular material is a classic example for this scenario: each grain is a perfect superconductor but has its own random phase. In such films, in order to achieve global phase coherence throughout the system, and by that, global superconductivity, Cooper pairs must hop from one grain to another. The ability of Cooper pairs to hop is based on two energy scales in the system: One is a Josephson energy, $E_j = I_c \Phi_0 / 2\pi$, where $\Phi_0 = h/2e$ is the superconducting flux quantum and I_c is the critical-current of the junction[21]. E_j is the energy of the coupling between the grains. The other energy scale is the charging energy of the grain $E_C = (2e)^2/2C$ where C is the capacitance of one grain[22]. The ratio E_C/E_j determines whether the system is superconducting or insulating; For $E_j > E_C$ Cooper pairs can tunnel between grains and the phase is well defined throughout the sample while for $E_j < E_C$ Cooper pairs are localized in the grains and phase coherence cannot be achieved.

Fig. 1.3 shows a set of R(T) curves for granular Pb films with increasing thickness[23]. The change of thickness is the tuning parameter which drives the system between superconductor and insulator phases.

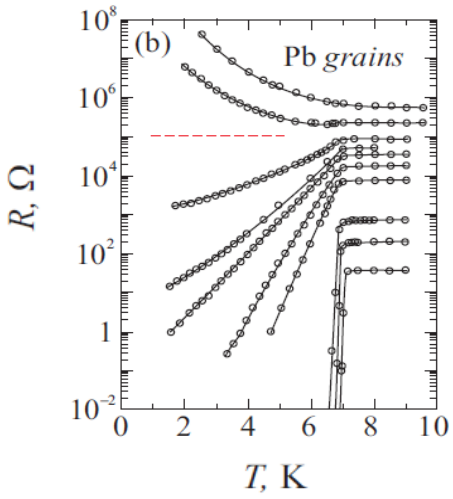

Figure 1.3: Resistance versus temperature for Pb films upon increasing their thickness (from top to bottom), exhibiting a superconductor-insulator transition. The films are granular, deposited directly onto SiO surface. The temperature of the superconducting transition in the becomes constant at a film thickness exceeding the critical one. The dashed red line is a separation between the superconducting films and the insulating films[23].

For the thinnest films, it is seen that as the temperature decreases, the resistance increases exponentially, i.e. an insulator phase. For the thickest film, the resistance drops to zero and a superconductor state is seen. Intermediate states characterized by long exponential tails, are seen between the superconducting and the insulating phases. Note that throughout the SIT a change in behavior is seen at the bulk T_c = 7.2K: a superconducting transition in the low-disorder films, a decrease in resistance in the intermediate disorder films, or a kink before the rise in resistance for high disorder films. Although disorder might also effects the transition, theoretically a simple and easy way to explain the granular Pb experiment is to consider E_C/E_j as the tuning parameter. For the insulating samples, the Josephson coupling is much smaller than the charging energy. Cooper pairs are localized on the grains and cannot tunnel from one to the other. In fact, the tunneling current between two superconducting grains, consists of two components: the superconducting Josephson current of Cooper pairs, and a single-particle tunneling. When Cooper pairs are localized, quasiparticle tunneling

becomes the controlling conduction mechanism[24]. At T_c, opening of the energy gap makes it more difficult to tunnel between islands, as in a superconductor-insulator-superconductor tunnel junction at voltages below the gap[25]. The tunneling becomes harder as the temperature decreases, resulting in increase of resistance. With gradually increasing thickness, the Josephson coupling energy becomes larger than the charging energy, transport of Cooper pairs between grains grows, and at T_c a decrease of resistance occurs, characterized by long exponential tails. Eventually, when the Josephson coupling overshadows the charging energy, a sharp transition occurs at the bulk T_c.

In the granular system we can therefore define two important critical temperatures. One is the temperature where Cooper pairs are formed T_ρ, and the other is the temperature where the superconducting phase is locked across the sample $T_\emptyset$, which may be equal to T_c (like in a BCS superconductor) or lower, and even zero for granular insulators. T_c is determined by the minimum of these two temperatures.

A conclusion which arises from the model is that traces of superconductivity exists not only in the superconducting phase, but also at the insulating phase. An indication for superconductivity in the insulator can be already seen in the transport measurements in Fig 1.3, where the uppermost curve changes its behavior abruptly at the critical temperature of the bulk material $T_c = 7.2$ Kelvin. Another example can be seen in Fig. 1.4 c, which shows dI/dV versus V curves of two InO films, one is a superconductor and the other is an insulator.

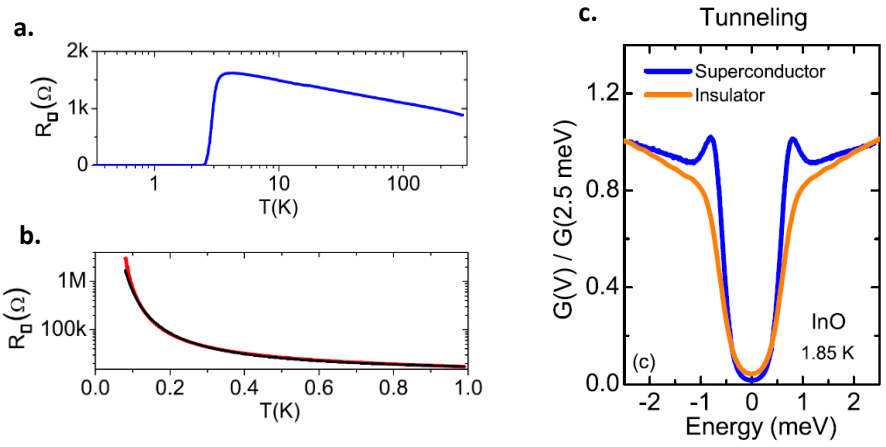

Figure 1.4: **a**. Temperature dependence of R□ for a superconducting InO film. **b**. Temperature dependence of R□ for an insulating InO film. **c**. Normalized tunneling density of state obtained at 1.85K for the superconducting film (blue) and for the insulating film (orange). Taken from[26].

These measurements show that a superconducting energy gap exists in both the superconducting and the insulating states of an amorphous film[26]. The existence of Cooper pairs in the insulating phases has been reported also at[16, 27, 28].

1.4. The bose metal phase

Since 1979, when the scaling theory of localization was proposed by Abrahams et al [29], and was supported by experiments, it became accepted that a 2D metallic state cannot exist in the absence of strong interactions. According to this theory, scaling arguments demonstrate that for non-interacting electrons, even weak disorder is sufficient to localize electrons at T=0. These ideas are expressed in terms of the so-called beta-function, defined as the logarithmic derivative of the conductance with respect to the length scale: $\beta(g) = \frac{d[\log(g)]}{d[\log(L)]}$. The behavior of $\beta(g)$ is well known in both large and small disorder degrees:

$\beta(g) = (d-2) - \frac{1}{g} + \cdots$ for $g \to \infty$

$\beta(g) \to -\infty$ for $g \ll 1$

and it seems reasonable to assume that between those two limits the function is continuous. Fig. 1.5 shows the results from this theory for the universal curve $\beta_d(g)$ in d = 1*;* 2*;* 3 dimensions.

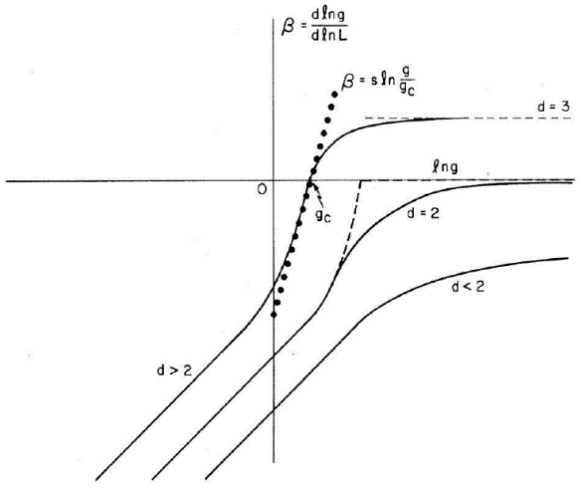

Figure 1.5: Temperature dependence of $\beta(g)$ as a function of g for different dimensions d = 1, 2, 3. For d = 2 the function $\beta(g) < 0$ so no metallic phase is expected[29].

In the upper half-plane β>0, the conductance increases with sample size L, which corresponds to a non-zero conductivity of a macroscopic sample at T=0 (metal). In the lower half-plane β <0, the conductance decreases exponentially with L and tends to zero for a macroscopic sample (insulator). Therefore, the transition from an insulator to a metal occurs upon crossing the point β =0. One can see that the transition between an insulator to a metal exists for d=3, whereas one-dimensional systems are always insulating at T=0[30]. In 2D there is no critical g_c where $\beta(g_c)$ =0, and β is always negative so that in all cases $g(L \to \infty)$[29]. In this case the system behaves as an insulator and cannot show a metallic behavior.

Despite the above, clues for an "anomalous" metallic state were observed in a variety of 2D disordered superconductors. An example is presented in Fig. 1.6: Christiansen et al measured a series of *a*-Ga films with different thicknesses. As can be seen, at low temperatures there is a wide region in which films shows a saturation of resistance, which indicates the presence of a metallic state[31].

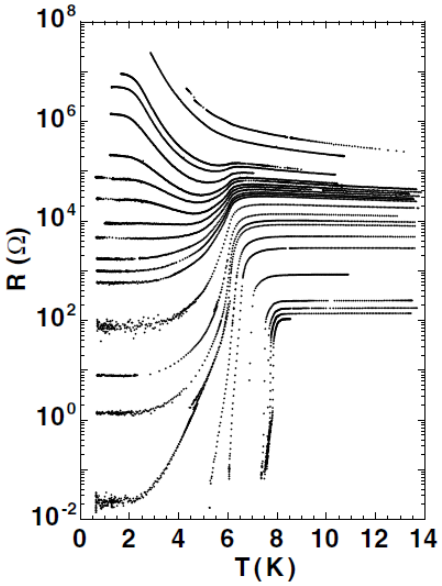

Figure 1.6: Evolution of the temperature dependence of the resistance for a series of Ga films. Film thicknesses range from 12.75 to 16.67 Å and increase from top to bottom. The plateau value of the resistivity increases as the distance from the superconducting phase increases[32] [Reprinted from[31]]

Since a metallic state in 2D is questionable, these observations require an explanation. Recently, Tamir et al[33] claimed that the presence of a metallic state in these 2D systems may be due to an experimental artifact. By measuring two different

superconducting films, they showed that the metallic state can be eliminated by filtering external radiation, as shown in Fig. 1.7.

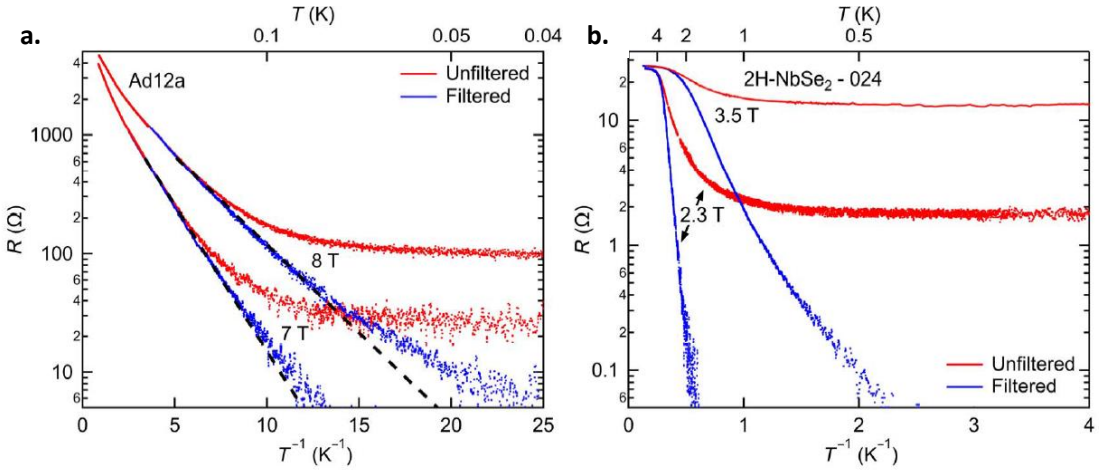

Figure 1.7: R versus T^{-1}obtained from: **a:** An amorphous InO (a:InO) film at B = 7 and 8 T, and **b**: a quad-layer 2H-NbSe2 at B = 2.3 and 3.5 T, respectively. Blue traces are measured with, and red traces without, filters. The top axis indicates the corresponding T's. The black dashed lines in **a** are guides to the eye, indicating activated behavior. The data were measured by applying a standard four-terminal lock-in technique with I_0 = 1 (a:InO) and 100 (2H-NbSe2) nA[33].

The figure shows R(T) measurements of two different materials at different magnetic fields, with and without filters. Without filters (red lines) the resistance shows a saturation at low temperatures, and with filters (blue lines) the resistance drops to zero as temperature is reduced. This led to the postulation that the anomalous metallic state that was observed is actually a suppressed superconducting state due to external radiation perturbations to which these films are extremely sensitive. Therefore, the reliability of metallic state measurements is still under debate.

Nevertheless, some measurements showing the "metal" state look more reliable. For example, most measurements of the metallic state in filtered periodic superconducting dots show signs of a metallic state. Two examples are shown in Fig. 1.8[18, 19]. In both cases, the studied system is a 2D periodic array of a superconducting material, and the tuning parameter is the coupling between the grains. One sample contains an array of square Al islands, connected by a gatable quantum well. The other system is a triangular array of Tin discs, connected by a graphene flake which serves as a proximity metal. As the gate voltage of the quantum well/graphene

is changed, the systems span over the superconducting regime, the insulating one, and between them a wide metallic regime, where finite resistances are measured at low temperature.

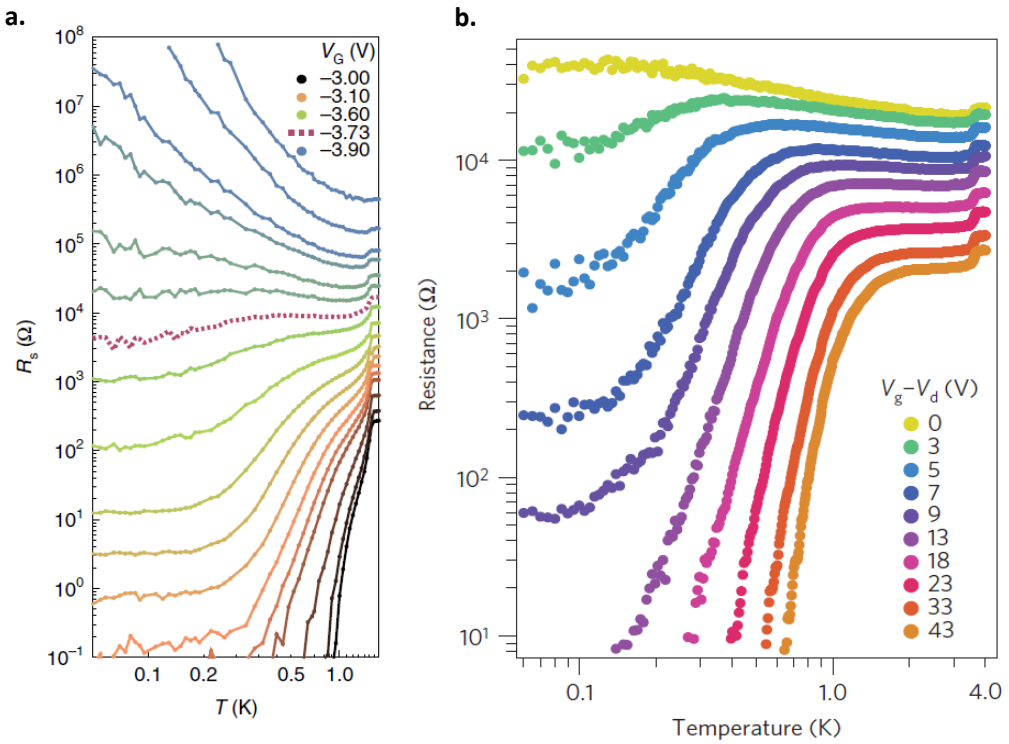

Figure 1.8: R(T) measurements of two 2D superconducting periodic arrays. **a.** Measurements of an array of square aluminum (Al) islands, connected by a gatable well. For the highest gate voltage (V=-3v) there is a transition to a superconducting state. For a range of lower gate voltages, the system exhibits a metallic state, with finite resistance that is saturated at low temperatures. For even lower gate voltages, one can observe the insulating regime of the system, with increasing resistance at low temperatures. Taken from[18]. **b.** Measurements of a triangular array of Tin (Sn) discs, connected by a gatable one-layer graphene. The resistance drops into a fully superconducting state for Vg-Vd>10V. A levelling-off to a gate-dependent finite value – a metallic state- is observed for 0<Vg-Vd<10V. Taken from[19].

Another example for measurements of an ordered granular system is shown in Fig. 1.9[34]. Here the system is a 2D Nb dots array coupled by an Au layer underneath. Measurements were conducted for different dots spacing, all of them showing superconductivity.

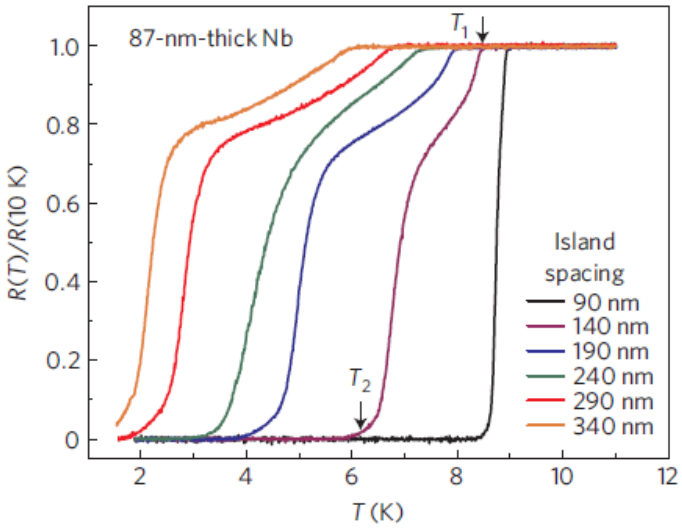

Figure 1.9: Temperature dependent resistive transition in arrays having different edge-to-edge spacing. Black arrows mark T_1 and T_2. The data are normalized to the resistance at 10K. All arrays show superconductivity. Taken from[34].

It can be seen that the resistance of the system drops to zero in two steps as the temperature is lowered: T_1 is the higher temperature drop, and T_2 is the lower. Both decrease as the island spacing increases. For all islands spacing, no metallic state is observed and the resistance falls to zero. We note, however, that all these measurements are of the superconducting phase only. The metallic state might appear between the superconducting and insulating phases of the system – at weaker coupled islands. An indication for that might be the saturation stage between T_1 and T_2 (except for the smallest spacing sample). As the spacing increases, the saturation stage becomes more dominant. This observation implies that a metallic state may be realizable for very weakly coupled islands.

1.5. Proximity effect

The proximity effect in an interface between a superconductor and a normal metal has been well studied both theoretically and experimentally. If the interface is of high quality, the superconducting order parameter amplitude, Ψ_0, does not drop abruptly from its full value to zero but rather varies smoothly across the interface[35, 36]. This has a twofold consequence. On one hand, there is a finite amplitude of the superconducting order parameter on the normal side extending a distance of the normal coherence length ξ_N, as a result of leakage of superconducting pairs and phase

coherence into the normal metal[37]. If the metal is dirty, with mean free path L_N shorter than the superconductor's coherence length, the decay length of Cooper pairs in the metal will vary as: $\xi_N = (\frac{\hbar v_F L_N}{6\pi k_B T})^{\frac{1}{2}}$ where v_F is the Fermi velocity of the metal[38]. Hence, a superconducting gap is created in the metal side near the interface. This phenomenon is called the *proximity effect*. On the other hand, Ψ_0 is suppressed on the superconducting side[39, 40] over a distance of the superconducting coherence length ξ_s, as a result of unpaired electrons from the normal metal diffusing into the superconductor and the superconducting gap decreases close to the interface. This phenomenon is called the *inverse proximity effect*. These two effects are influenced by three parameters: the transmission of interface between the superconducting material and the metal, t, the decay length of Cooper pairs in the normal state ξ_N and the superconducting coherence length ξ_s. The effect of metal-superconductor proximity is schematically summarized in Fig. 1.10, which shows the superconducting gap near the interface.

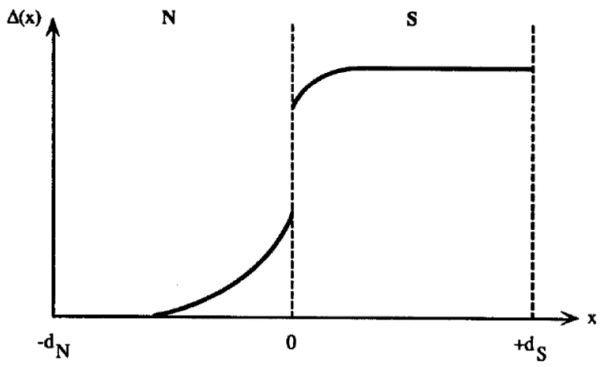

Figure 1.10: Superconducting gap as a function of position. The interface between the normal and the superconducting regions is at x = 0 with the normal metal to the left and the superconductor to the right. A clear discontinuity is seen across the interface which indicates a less-than-perfect interfacial transparency[41]. Taken from[42].

An experiment showing both sides of the proximity effect was conducted in granular Pb films. The addition of a metallic Ag layer on top of an insulating granular layer of Pb induced superconductivity. R(T) curves of this proximity effect experiment are shown in Fig. 1.11.

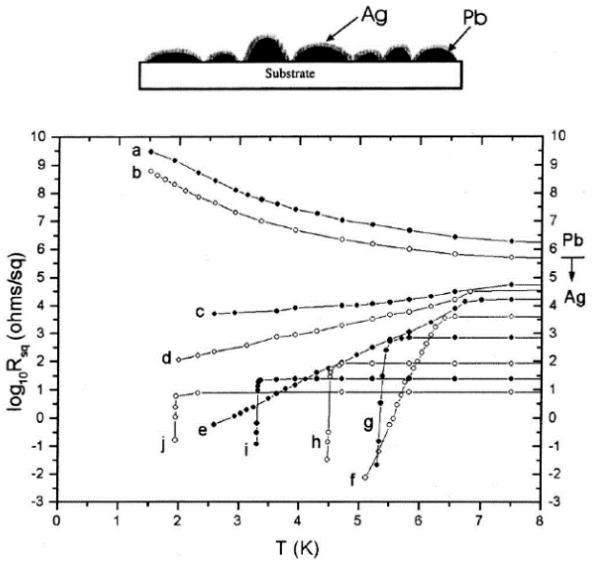

Figure 1.11: Sheet resistance as a function of temperature of Pb/Ag layers. Curves a and b are for Pb layers, curves c-j are for the Pb layer from b with incremental addition of Ag. Taken from[43].

In this experiment, an insulating granular Pb is deposited on a substrate (Curves a and b). The following stages are for the gradual addition of silver on top of the Pb. Although Ag is a non-superconducting material, cooper pairs can tunnel between the lead grains through the Ag, enabling phase coherence between the grains and a global superconductivity. As layers of Ag are added, the transition to a superconducting state is gradually sharpening, as shown in curves c-f. This is attributed to the increase in phase coherence between the grains. At later stages (g-j), the transition is very sharp, however T_c decreases due to the inverse proximity effect.

1.6. Andreev reflection and the BTK model

A microscopic view of the superconducting proximity effect is the Andreev reflection (AR). Andreev (1964) demonstrated how single-electron states of the normal metal are converted into Cooper pairs[44]: when an electron from the normal metal, with energy $E<\Delta$ tries to pass through the interface and to enter the superconductor it cannot continue through as a quasiparticle, since the excitations in a superconductor have a minimum energy of Δ. In this case, the electron reflects as a hole in the normal metal

while simultaneously adding a pair to the condensate in the superconducting metal. If the electron carries ev_F of current (v_F is the Fermi velocity), then $2ev_F$ of net current is flowing because the returning hole carries (-e)(- v_F). Of course, to conserve current, the electron pair also carries $2ev_F$. At low voltage, eV <Δ and T=0, all of the electrons impinge upon the gap and Andreev reflect, so that twice as much current flows as in the normal state[45].

The consequences of AR on the current voltage characteristics of a S-N junction were studied in detail in the BTK theory[46]. If there is a tunnel barrier at the interface, electrons undergo a combination of normal reflection and AR. As the strength of the barrier is increased, normal reflection begins to dominate[45] and the probability of AR is gradually suppressed. The barrier strength was characterized by a simple parameter Z ranging from 0 for a perfect metallic contact to ∞ for a low transparency tunnel barrier. According to this definition, the transparency is t = 1/(1 + Z^2). An illustration of dI/dV vs V curve for different z values at T=0 is shown in Fig 1.12.

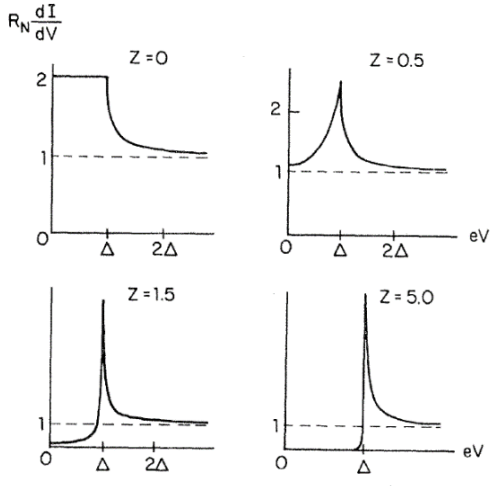

Figure 1.12: Differential conductance vs voltage for various barrier strengths Z at T=0[46].

For Z=0 and eV <Δ, all the electrons undergo AR. As Z increases, normal reflection begins to dominate, the excess current (proportional to the fraction Andreev reflected) gradually disappears, and the I-V curve becomes similar to that of an ideal tunnel junction[45]. Z=5 represents a case when nearly all the electrons experience only normal reflection (a tunnel junction)[46].

The Andreev process is significant when the transparency of the barrier is high[47]. A physical barrier is not the only source for normal reflection. Since usually the S and N are different materials, they have different V_F. Fermi velocities will be different in each bank. This impedance mismatch results in some normal reflection, even with no physical barrier present. Fig. 1.13 illustrates a typical result for a pure metallic I-V curve, where the ratio of the Fermi velocities of the two electrodes is defined as $r = V_{FN}/V_{FS}$ and its value is r =$\sqrt{2}$. One can easily see that this effect is exactly reproduced by simply shifting Z to a higher effective value while setting the Fermi velocities equal[45], according to the following equation:

$$Z_{eff} = [Z^2 + (1 - r)^2/4r]^{1/2}$$

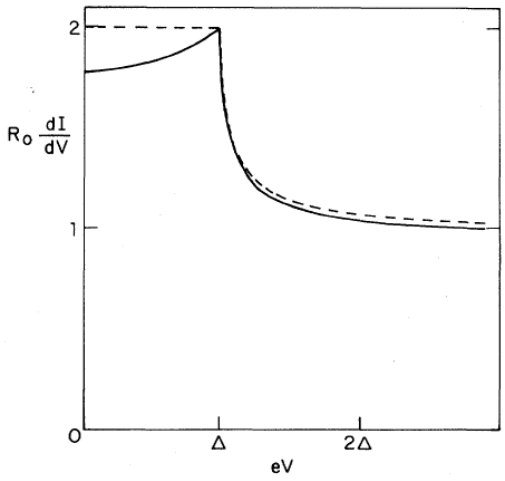

Figure 1.13: dI/dV vs V at T=0 for the pure metallic (Z=0) case. Dotted curve assumes the Fermi velocities are equal in both metals; solid curve assumes the ratio r of Fermi velocities is equal to $\sqrt{2}$. Latter curve is mathematically equivalent to one generated assuming equal Fermi velocities and Z=0.175[45].

In view of this result, the impedance mismatch is included simply as a shift in the measured Z.

2. Goals and aims

In this work, we would like to shed light on the possible 2D "Bose metal" phase that has been proposed in recent years to exist between the insulator and superconductor phases. Since the existence of a metallic state in 2D is theoretically questionable, this subject requires attention.

We chose to focus our research on ordered granular systems. In this kind of systems, the disorder is very small, thus, enabling us to study an SIT that is tuned primarily by the coupling energy and governed by Ec/Ej. In addition, this type of systems shows prominent presence of a metallic phase.

In this work we conduct measurements on periodic ordered superconducting arrays, in an attempt to study the effect of a barrier between the superconducting grains on the bose metal state. For that purpose, we examine different barrier strengths, by fabricating two types of samples: one with a physical barrier between the grains – an oxide layer, and one with a clean interface. A comparison between these two cases can provide some insights on the barrier's influence on the anomalous metallic state appearance.

3. Experimental methods

3.1. Quench condensation

Quench condensation is a thin film deposition technique employing physical vapor deposition on samples held at cryogenic temperatures. It allows the study of ultra-thin films as a function of thickness by *in-situ* sequential deposition. The uniqueness of the quench condensation technique is that the substrate is kept inside a vacuum chamber and at low temperatures due to thermal coupling to a cryogenic heat bath. This means that the evaporated atoms that adhere to the surface become rapidly immobile, as their kinetic energy is transferred to the heat bath. Despite this rapid freezing process, nucleation sites may be present in the substrate which attract additional nearby atoms, resulting in a granular film on silicon substrates. One may add a wetting layer of Sb or Ge before performing the quench-condensing. This makes the atoms adhere better to the surface and results in uniform rather than granular films.

The setup consists of a tungsten wire, which is wound to form a conical helix shape and is used as the evaporation boat (Fig. 3.1). A small granule of the material to be deposited is placed inside this cone. The feed-through are inserted into a vacuum chamber and connected to a current source. Current is driven through the boat to the point where the material melts. This ensures that when moved and handled later the granule doesn't fall out of the boat. The setup of the evaporation boat is connected to the low-temperature cryo systems. A picture of our evaporation system is shown in Fig 3.1.

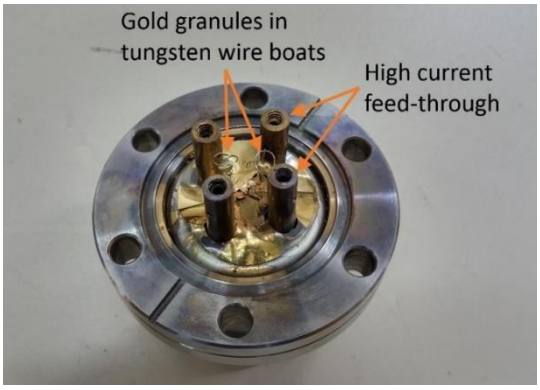

Figure 3.1: The physical vapor deposition source used in our measurements. The four metallic columns that feed the current for the evaporation boats exit the chamber without breaking the vacuum inside.

In our study we use quench-condensation for adding a metallic layer on top of a superconducting dots array. The studied samples are arrays of Nb dots, coated by quench-condensed layers of metal (Au or Ag) for increasing the coupling between the dots.

3.2. Superconducting dot array preparation

Arrays of superconducting dots were fabricated using different methods. The Nb was deposited by sputtering, causing the dots to form high edges, as shown in Fig 3.2.

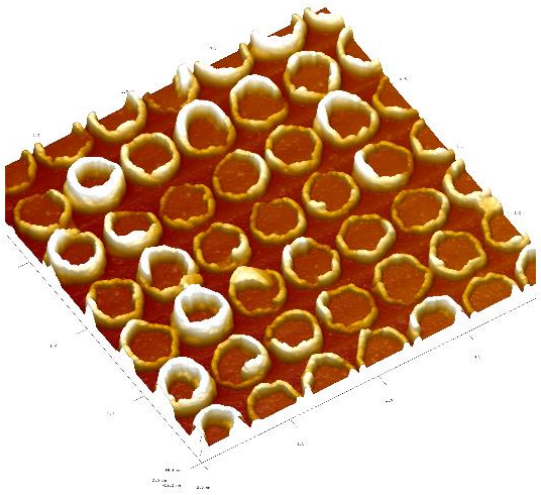

Figure 3.2: Nb dots array with dot diameter of 200 nm and 30 nm thickness. Deposited by sputtering.

Since ultra-thin layers will be evaporated on top of the dots, these high edges are problematic since they may prevent the layers from being continuous. In order to prevent that, we used the following scheme: An array of Al dots is fabricated on top of a 30nm Nb wafer. Then, the Nb is etched away, using a Reactive Ion Etcher (EIR). The Al dots protect the Nb underneath from the etching process. As a result, the wafer is clean from Nb, except under the Al dots. Finally, the Al is removed with AZ351. An illustration of this scheme is presented in Fig 3.3.

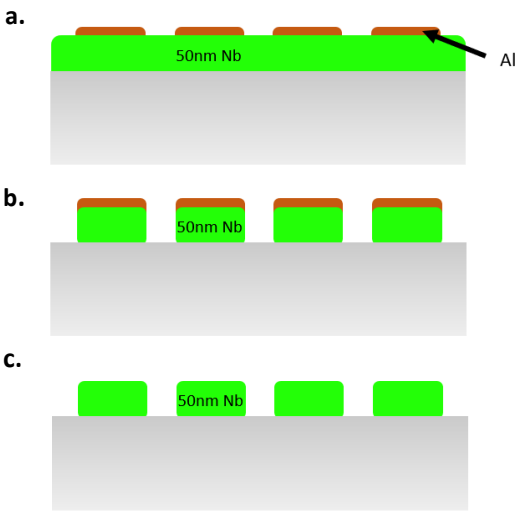

Figure 3.3: The different steps of dot array fabrication, using Al dots cover. **a.** Aluminum dots are fabricated on top of the Nb wafer. **b.** The Nb is etched. Nb is left only under the Al dots. **c.** The Al covers are removed with AZ 351.

Later, the evaporation method of Nb was changed to e-beam evaporation and the high edges that are created by sputtering were prevented.

However, even by using the scheme presented above, the figures are still characterized by sharp edges after lift-off. These may be problematic as well, since they may create a "shadow effect" for evaporation and prevent continuity of the film. An illustrated is shown at Fig 3.4.

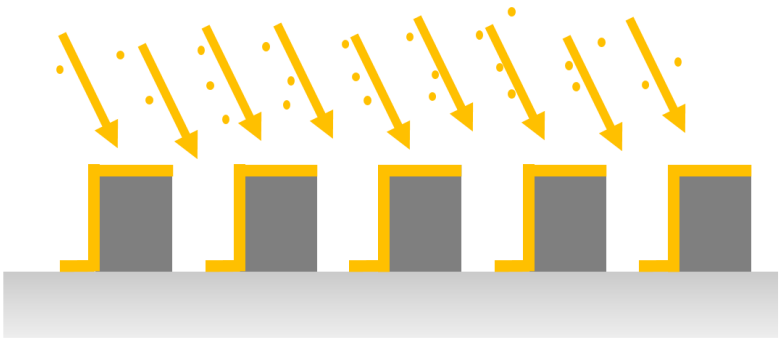

Figure 3.4: An illustration of shadow areas, as a result of an angled evaporation on sharp edged figures.

In order to prevent this we fabricated dots using double-layer photoresist. However, because of small spacing between the dots, the resist collapsed and didn't survive the process. Therefore, the method was changed to a regular one-layer photoresist. In order to overcome the shadow effect problem, a thin layer of metal was fabricated underneath the dots. The metal's thickness (which affects its resistance) is chosen in such a way that the metal will provide some initial coupling between the dots, but the system will still be in the insulating phase. The dots were fabricated by photolithography, using a Heidelberg instruments MLA 150 machine, or by e-beam lithography, using a CABLE-9000 scanning electron microscope. Pictures of dots array prepared by different methods are shown in Fig 3.5.

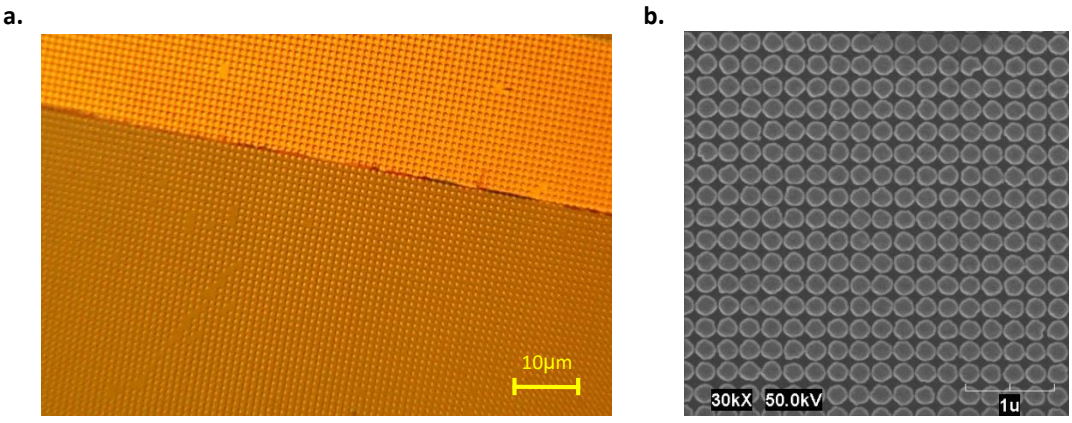

Figure 3.5: Nb dot arrays, fabricated by different methods. **a**. An array made by photolithography. Dot diameter is 1 µm. Picture is taken by an optical microscope. **b**. An array made by e-beam lithography, with Al dots fabrication and etching process. Picture is taken by a SEM microscope. Dot diameter is 250 nm.

The dots were made with diameters ranging from 250 nm to 1 µm. In the results section it will be established that the size has no effect on the system's T_c.

3.3. Sample preparation

In order to measure the sample's resistance, Au contacts (4nm Ti and 40nm Au) were written by photolithography, using Heidelberg instruments MLA 150 machine, as can be seen in Fig 3.6.

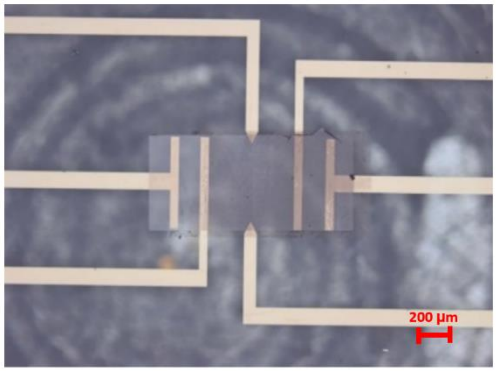

Figure 3.6: Nb dots array on top of an Au square, connected to 4 probe leads. Picture is taken by an optical microscope.

In order to measure the SIT and check the influence of the barrier between the dots, we prepared two types of samples.

The main difference between the two samples is the presence/absence of an oxide layer on top of the Nb dots: Nb gets oxidized when exposed to air, and an oxide layer is formed between the dots and the metallic layer on top. In order to have as clean interface as possible between the dots and the layer above, in one kind of samples the oxide on the dots was etched prior to evaporation of a very thin layer of metal, without breaking the vacuum in between.

3.3.1. Type A (Oxidized):

First, Au contacts are fabricated to define 4 probe geometry. Then, a square of a thin Au layer is made at the measurement area (4nm Ti for a better adhesion and 4nm Au) for initial coupling between the dots. Both the contacts and the square are made through photolithography process, by Heidelberg instruments MLA 150 machine. On top of the Au square, the ordered granular array is added. The sample is exposed to air in the process, causing the Nb to oxidize. An illustration of the sample is shown in Fig. 3.7.

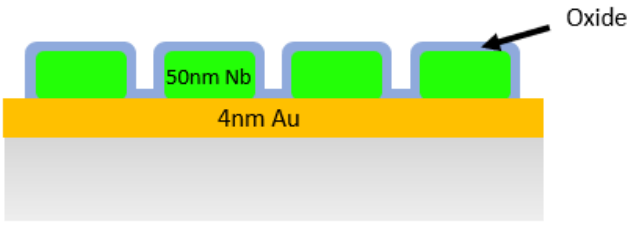

Figure 3.7: A side look on type A. The Nb gets an oxide layer after exposure to air.

3.3.2. Type B (Non-oxidized):

First, the dots array is fabricated. A set of Au contacts is fabricated to define a 4-probe geometry by a photolithography process. Here also an oxide layer naturally grows on top of the Nb. This oxide is removed by etching a few nm from the dots surface and then, without breaking vacuum, a thin layer of Au is evaporated *in-situ* on the measurement area to prevent re-oxidation. The process of fabrication is shown in Fig. 3.8.

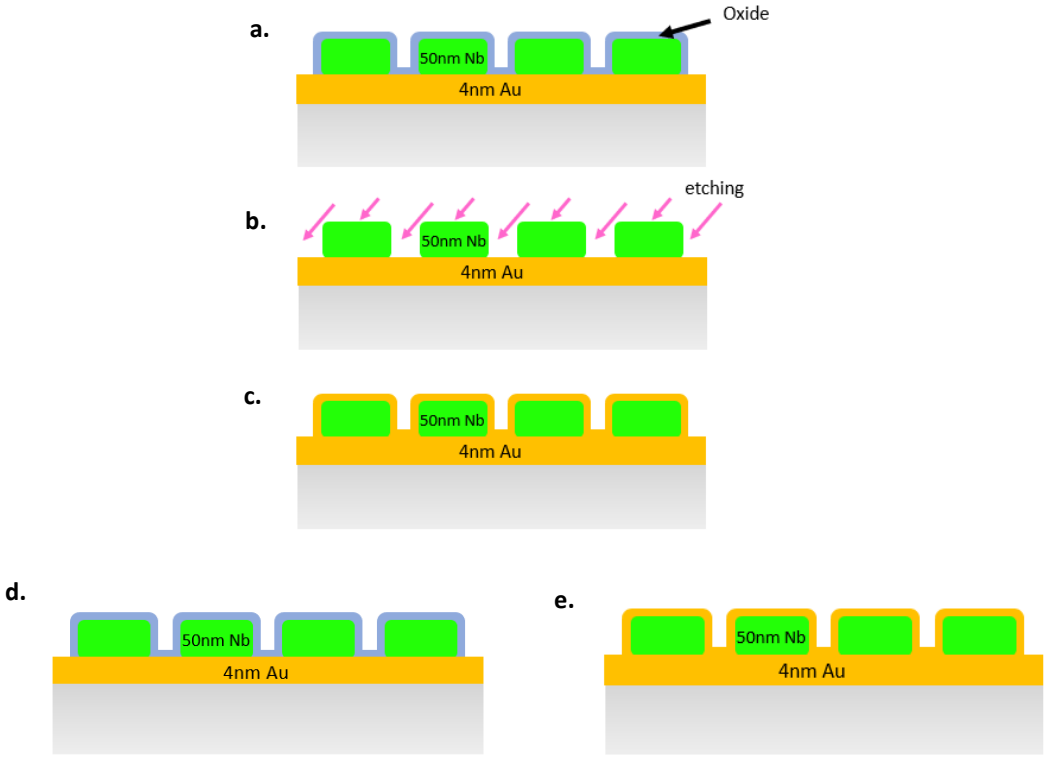

Figure 3.8: The different steps of oxide movement. **a.** The Nb is exposed to air. As a result, an oxide grows on top of the dots. **b**. The oxide is etched away. **c.** The sample is evaporated in situ with a thin layer of Au which prevents an additional oxidation. **d-e**: Models of the two different sample types: **d** is type A and **e** is type B.

Pictures of a type B (Non-oxidized) sample is shown in Fig. 3.9.

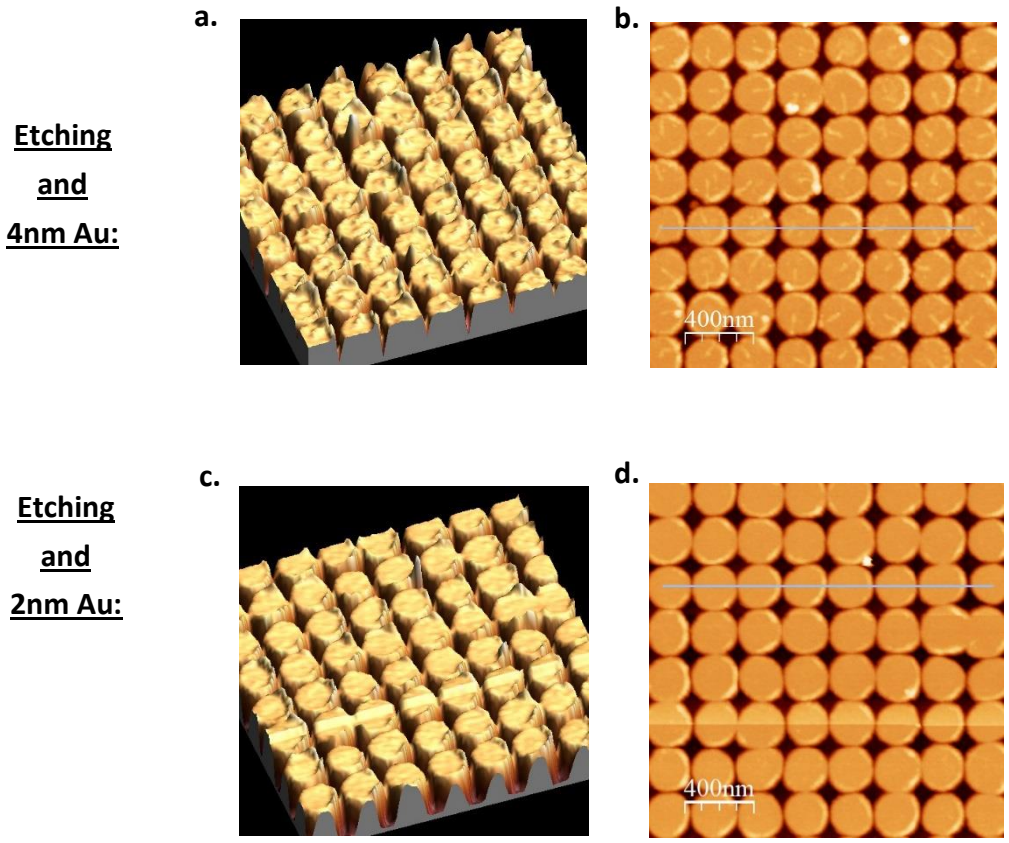

Figure 3.9: AFM photos of dots array in 2D and 3D, fabricated on the two discussed samples before the Au evaporation on top. **a** and **b**: Photos of the sample evaporated with 4 nm Au layer. **c** and **d**: Photos of the sample evaporated with 2 nm Au layer.

For both kinds of samples, after the preparation steps above, additional metallic layers are added on top by a quench condensation technique for strengthening the coupling of the dots and transiting the sample to its superconducting state. After each evaporation, a measurement is taken. A scheme of the quench-condensation process for the two samples is presented in Fig. 3.10.

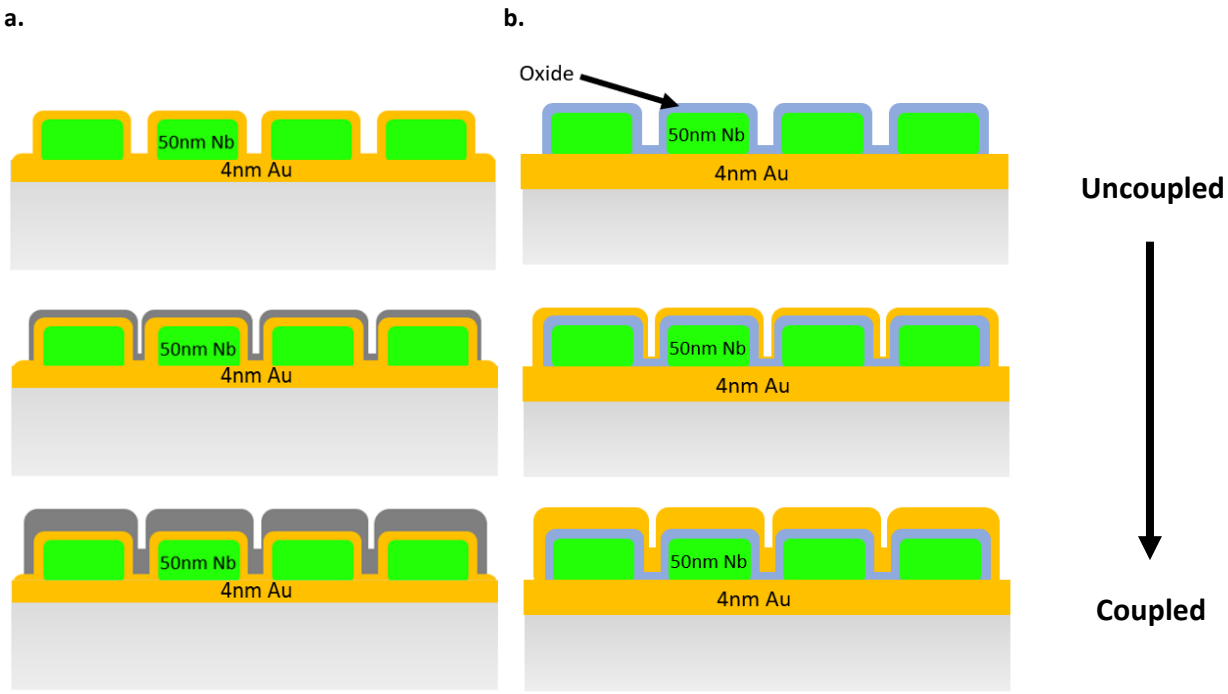

Figure 3.10: The different steps of metal evaporation on top of the samples during quench condensation process. Au evaporation for type A, Ag evaporation for type B. **a** is for type A and **b** is for type B. As the metal thickness increases, so the coupling between the dots increases.

More than 30 different samples were fabricated by using different methods. 8 of them were measurable, but only one sample from each type yielded comprehensive results.

3.4. R(T) measurements

We measured the resistance as a function of temperature, using 4 probes and lock-in amplifier techniques. The two measurement systems are: a ^{3}He system, capable of base temperature of 300mK and an optical cryostat, which is capable of base temperature of 1.8K. All the electrical wires pass through a three-stage low pass R-C filter. For this we used SMD resistors (150 Ω, Vishay TNPW thin film) and capacitors (22 nF, AVX COG) on a custom-made PCB. The cut-off frequency f_c for the filters were 50 kHz. A schematic drawing of the filter and a picture of the measurement system are shown in Fig 3.11. The gold plating at the bottom of the PCB was connected to ground.

a.

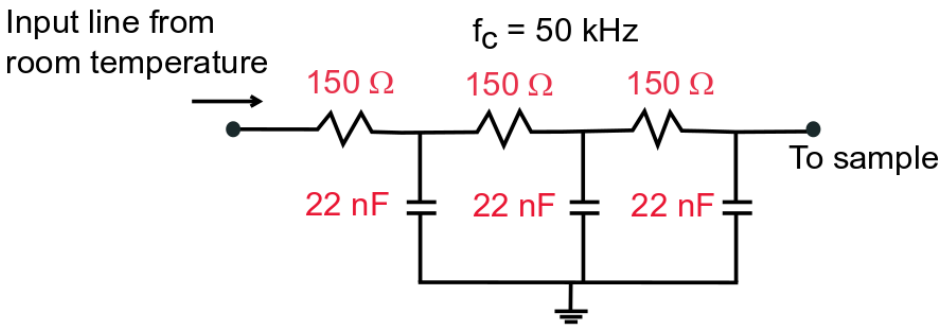

b.

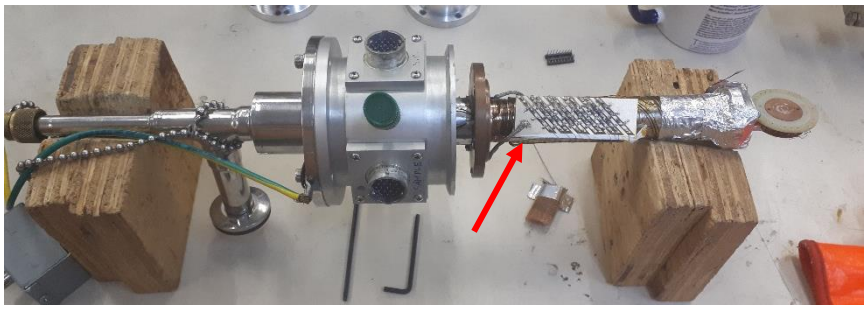

Figure 3.11: **a**. Schematic of the filter. Three stage R-C filter was used to cut off the higher frequency. The filters were mounted on the system. **b**. A picture of the cooling system. The red arrow shows the filters.

4. Results

4.1. Sample characterization

In order to characterize the dots, the first check was to verify that each grain is an individual superconductor. An R(T) measurement would provide us an information about the global superconductivity, but not about each grain. Therefore, we used scanning SQUID (at Kalisky's lab. They performed the measurements for us) in order to measure local susceptibility. A susceptibility image of the dots is shown in Fig 4.1. An ideal superconductor screens the magnetic field completely at fields lower than the critical field. Hence, the magnetic response should be negative for superconducting areas (white color, according to the scale bar). Since the picture shows a pattern of a white dot array, it verifies the fact that each dot becomes a superconductor.

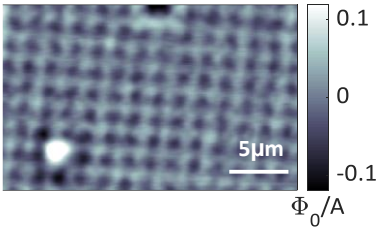

Figure 4.1: The magnetic response to a locally applied field of a Nb dots array. Dark areas are negative signals and white are a positive one, which are considered as superconducting.

Next, we checked the effect of the dots' size on the T_c of the system. For that purpose, an array of Nb rectangles with different sizes was fabricated and scanned by the SQUID. The rectangles lengths are 1-5 µm with a width of 5 µm. A graph of susceptibility versus temperature of different rectangles sizes is shown in Fig 4.2.

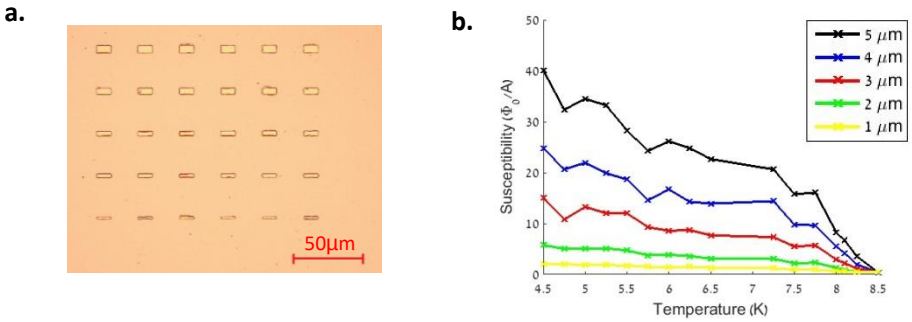

Figure 4.2: **a.** An array of 50nm thickness Nb rectangles. The width of the rectangles changes between lines, starting at 5µm at the upper line and ending at 1µm at the lower line. The length of all rectangles

is 5 μm. The photo was taken with a microscope. **b.** Susceptibility versus temperature for different rectangles' sizes.

The susceptibility increases as the temperature decreases, in coordination with superconductivity's strengthening. As can be seen, for all different sizes the susceptibility rises from zero at the same temperature of ~8.5K. In other words, superconductivity appears at the rectangles at the same temperature.

Moreover, measurements of resistance versus temperature of dots with much smaller diameter of 170 nm and 250 nm are presented at Fig. 4.3. The dots were fabricated by e-beam lithography.

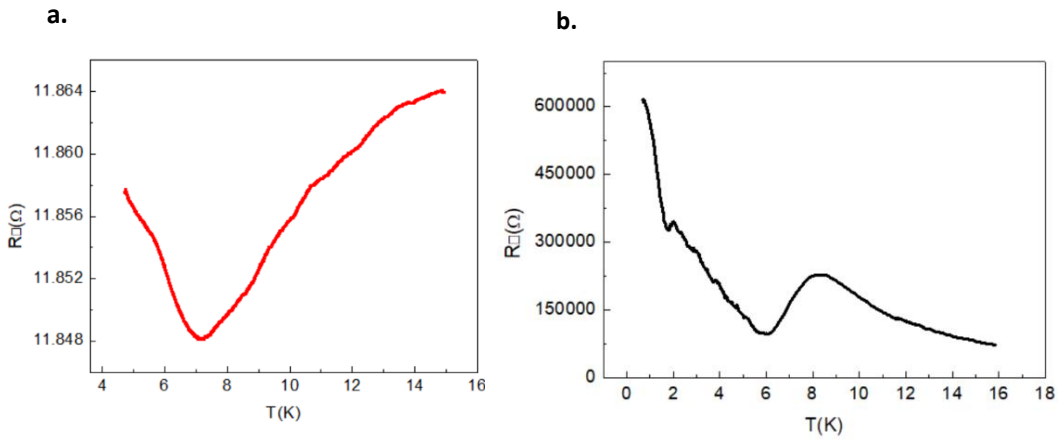

Figure 4.3: R(T) measurements of three different samples of dots array. **a.** A sample with dots' diameter of 170nm. **b.** 250 nm.

The initial desired coupling level between the dots is difficult to control, hence the samples have different coupling level, causing different behaviors of resistance as function of temperature curves. Nevertheless, despite the smaller size compare to the rectangles in Fig 4.2, the samples show T_c which is similar, at 7-8 K. We conclude that the diameter of the dots has no influence on the T_c of the system, nor has the fabrication methods – e-beam vs photolithography.

4.2. R(T) measurements:

In this section we present and compare the results of type A samples (Oxidized) and type B (Non-oxidized). The quench condensed metallic layer was Ag for type A and Au for type B. Past experience in our lab indicate that Ag and Au have the same effect when being used as a top layer.

Fig 4.4 presents measurements of resistance as a function of temperature of the two samples for different coupling metal thickness, evaporated on top of the sample using quench condensation technique. For clarity, the resistance values are normalized according to the resistance at T=10K.

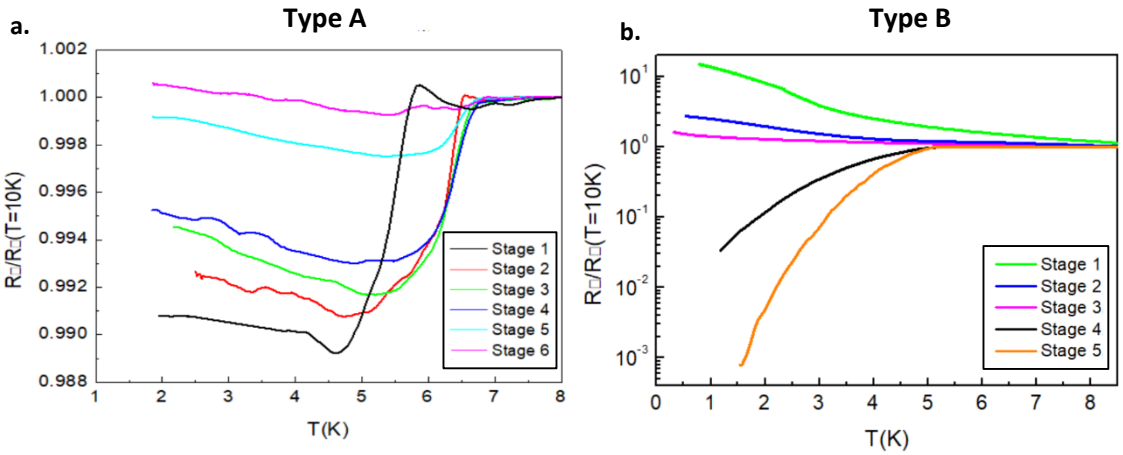

Figure 4.4: A normalized resistance R(T)/R(T=9.6K) vs temperature curves of the two samples. **a.** R(T) of type A (Oxidized) sample. Each plot represents a different stage of Ag evaporation, starting from stage 0 (black) to stage 6 (pink). **b.** R(T) of type B (Non-oxidized) sample. Each plot represents a different stage of Au evaporation, starting from stage 0 (green) to stage 5 (orange).

As can be seen in sample B, as a function of the Au thickness, the system transits from an insulator to a superconductor.

In sample A, on the other hand, the system wasn't driven through the whole SIT. However, at the measured region, for all evaporation steps there is a small drop of resistance at T_c between 5.4-6.5 K, followed by a saturation. Fig 4.5 represents the change of the resistance drop as a function of resistance at T=8 K.

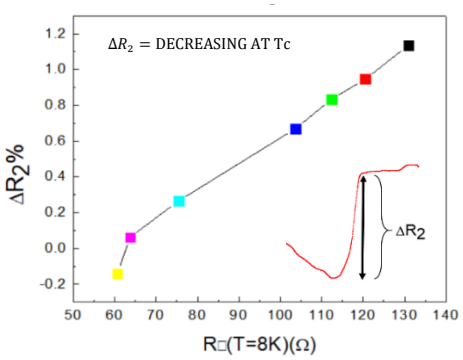

Figure 4.5: The relative resistance drop (in %) – defined as ΔR2 - divided by the resistance value at T=8K as a function the resistance at T=8K. **On the inset**: An illustration describing the definition of ΔR2.

It is seen that the value of the relative resistance drop decreases as the thickness increases.

T_c is defined as 50% drop in the normal state resistance at T=8K, and for each evaporation step T_c was extracted. T_c of the two samples are shown in Fig 4.6.

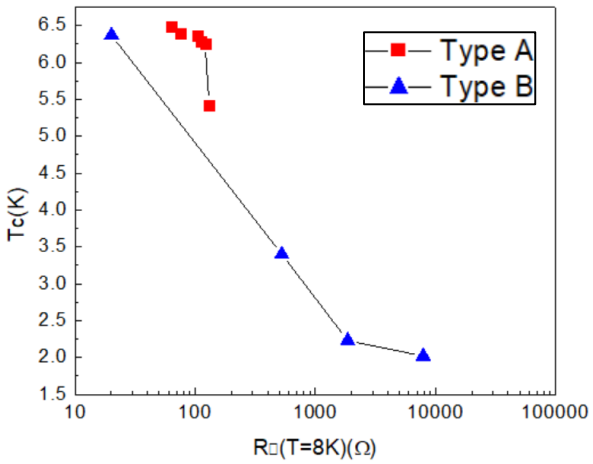

Figure 4.6: T_c as a function of resistance at T=8K for type A (red) and type B (blue).

As can be seen, the T_c of type A (dots' diameter of 1μm) is slightly increasing after the first evaporation and then barely changes from 6.4 K. For type B (dot diameter of 250nm) as more evaporation steps are made – and the metal layer's thickness increases - T_c increases. Note that for the two samples, all the T_c 's are smaller than the T_c bulk of Nb – 9.2K. We assume that for large dots' size, T_c will reach ~8K like the T_c of the bigger dots, as shown in Fig 4.2 b.

Both of the samples were affected by the change of thickness of the metallic layer which was evaporated on top of the systems. However, the measurements show a difference between the two: the sample with an oxide between the dots and the upper layer shows a resistance saturation after the resistance drop at T_c, while the sample with a clean interface didn't exhibit such a resistance saturation.

5. Discussion

In our experiment, we compare between two kinds of samples: one sample, type A, has an oxide layer between the dots and the metallic layer, and the other sample, type B, has a clean interface. As seen in Fig 4.4 a, most of the measured resistance of type A is due to the Au layer under the dots, as the resistance drop in the first curve resulted by the superconducting Nb is less than 1.2% (Fig 4.5). As more Au is added, its impact is larger and the effect of the superconducting current is further reduced. As a result, the size of resistance drop decreases. In type B measurement, as more Au is evaporated, ξ_N increases. Hence, the grains' coupling increases and it will be easier for Cooper pairs to hop between grains. As a result, the effective size of the grains becomes larger, resulting in higher T_c of the system, as can be seen at Fig 4.6. The smaller grains sizes cause the T_c to start at much lower values, compare to the other sample (Fig 4.6). On the other hand, in type A measurements, because of the big amount of Au underneath the dots, the initial coupling level of the sample is high and T_c is barely changing as more Ag is added.

As noted above, sample A shows a saturation of resistance which implies a metallic state, while sample B shows a direct transition between insulator to a superconductor, without a metallic state signs.

In order to explain these results, let's examine the experimental system: in order to achieve global superconductivity in a system of superconducting dots embedded in a metal, two things should be considered. The first is the transparency t of the interface between the metal and the superconducting dots. In order to enable Cooper pairs to transit from the superconductor to the metal, the transmission between the two materials should be high. Second, the ratio between ξ_N to the metal's length - L. Superconductivity penetrates the normal material region to a distance of ξ_N. If the length of the normal material is larger than ξ_N, Cooper pairs cannot tunnel between the grains, i.e. a global superconductivity isn't achieved.

Let's consider three scenarios of system with superconducting dots embedded in a metal: 1. The metal is in good contact with the superconducting dots, and the transmission is good. 2. The interface isn’t "clean" - an oxide layer or other barrier exists in between the metal and the superconducting dots which effects the transparency *t*. 3. There is a good interface but the ratio between the fermi velocities of the metal and

the superconducting dots is significant, which affects the transmissivity of the interface as a barrier [46]. The last two cases are equivalent. A scheme of the different scenarios is presented Fig. 5.1.

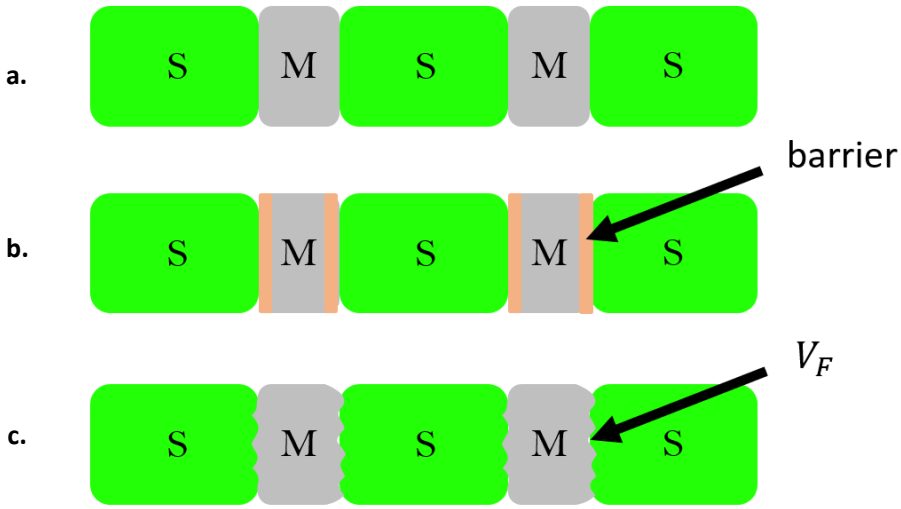

Figure 5.1: Three different kinds of interfaces between the superconducting and metal materials. **a**: A direct and clean interface. **b**. An interface with a barrier. **c**. A clean interface but there is a difference between the fermi velocities of the two materials.

The first scenario of a high-quality interface is realized in the cases of our type B (Non-oxidized) sample (Fig 4.4 b), and in InO measurements of Tamir's group (Fig 1.7).

Type B sample has a clean interface between the Nb and the Au above, without an oxide in between. The fermi velocities of the two materials are:

$$V_F(Au) = 1.4 * 10^6 \frac{m}{s} \qquad V_F(Nb) = 1.37 * 10^6 \frac{m}{s}$$

As can be seen, the velocities are very close, making the interface clean and as a result, the transmission is high. Changing the metal thickness tunes the coupling between the dots and changes the ξ_N of the metal. The system changes directly from an insulator to a superconductor and no metallic state is observed.

Despite the fact that InO films are fabricated as homogeneous films, it has been demonstrated that they are electrically granular: within the seemingly homogeneous matrix separated regions of superconducting and normal-state electrons coexist. In this case, there is a clean interface between the superconducting and normal regions. Moreover, both the metal and the superconducting regions are made of the same material. The fermi velocity might change between different regions, but not significantly. Hence, as in our type B samples, the transmission is high. These systems didn't show a metallic state.

The second scenario is realized in the case of our type A (Oxidized) sample (Fig 4.4 a). The sample has an oxide layer between the Nb and the Ag above, which reduces t. Like type B, the metal thickness tunes the coupling between the dots and effects the system behavior. In this case, signs of a metallic state are shown, as the resistance saturates at low temperatures for all different Ag thicknesses.

The third scenario is relevant for the measurements of Tin dots on top of graphene (Fig 1.8 b), and Al squares on top of a semi-conductor (Fig 1.8 a). In both cases, there isn't a physical barrier between the dots and the graphene or the semi-conductor. However, the fermi velocity is different between the dots and the substrate, which effects the transmission. The fermi velocities of the materials are [48, 49]:

$$V_F(Graphene) = 0.85 - 1.73 * 10^6 \frac{m}{s} \qquad V_F(Tin) = 1.9 * 10^6 \frac{m}{s}$$

$$V_F(\mathrm{InGaAs}) = 0.07 * 10^6 \frac{m}{s} \qquad V_F(Al) = 2.03 * 10^6 \frac{m}{s}$$

A significant difference of fermi velocities exists between the graphene and the Tin, and between the InGaAs and the Al. In both cases, signs of a metallic state were measured.

A summary of the different experiments representing different types of interfaces, is shown in Fig 5.2.

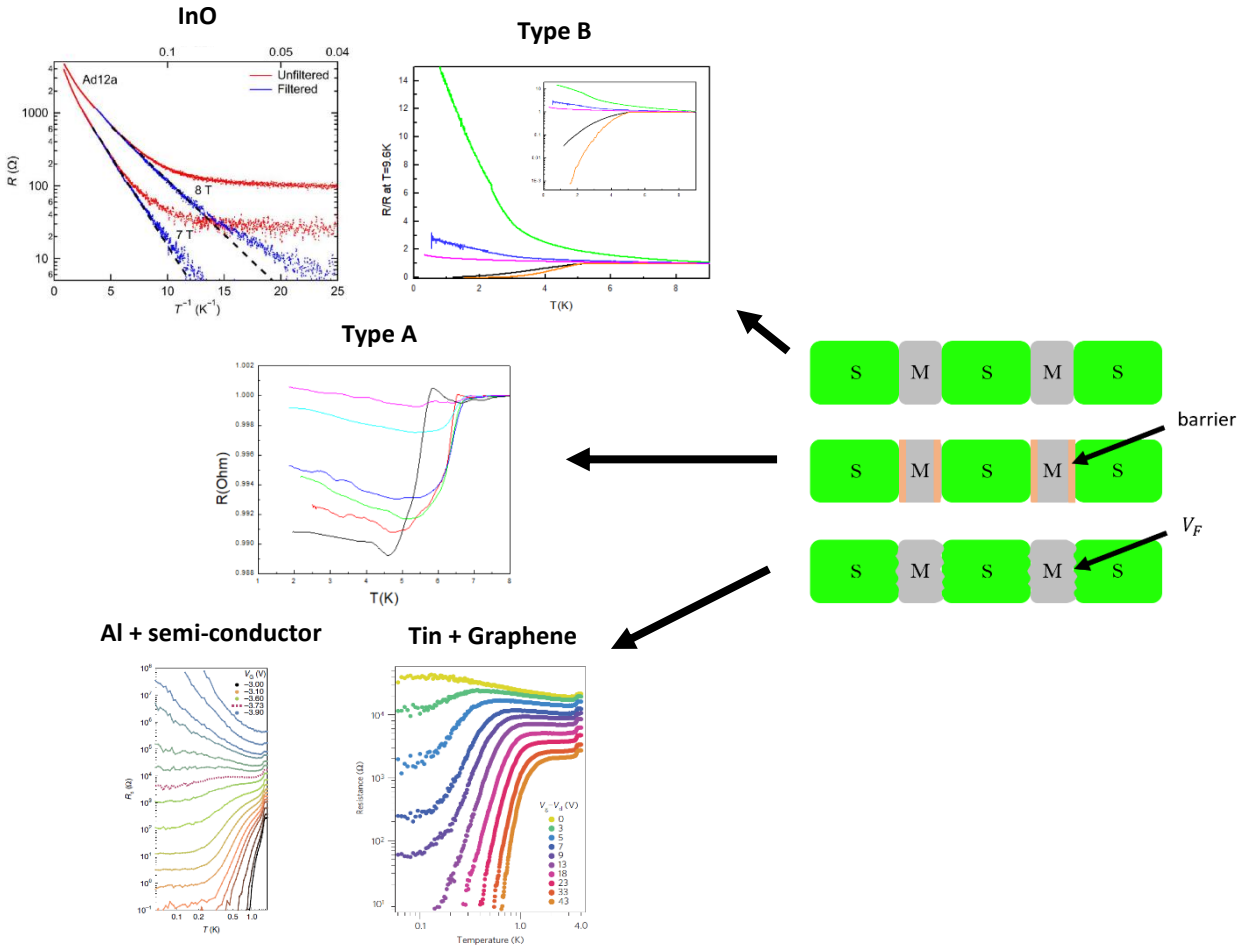

Figure 5.2: On the right: the three different kinds of interfaces between the superconducting material and the metal. On the left: measurements of different systems, each one connected to the appropriate kind of interface.

As can be seen, when the interface between the superconducting material and the metal is of good quality, the system doesn't show a metallic behavior. On the other hand, when the interface has a barrier – a real barrier or a large fermi velocities mismatch – a metallic state appears.

6. conclusions

Theoretically, metallic states shouldn't exist at zero temperature in two-dimensional systems. Since an anomalous metallic state has been experimentally observed even when approaching zero temperature, an explanation for this phenomenon is required.

In this work, in order to characterize the metallic state appearance, we studied the effect of a physical barrier between the superconducting grains on the presence of the bose metal phase in 2D ordered granular systems. We fabricated two types of coupled superconducting dot arrays: one with an oxide layer between the grains, and one with a clean interface. The measurements showed signs of a metallic state for the oxidized sample, while the clean-interface sample showed a direct transition between a superconductor and an insulator.

Based on our measurements as well as those of other groups, our conclusion is that systems with a clean interface between the superconductor and the coupling medium show a direct transition between an insulating state to a superconductor, while systems with bad coupling between the two materials usually show signs for a metallic state. We suggest that the metallic state appears when the transmission of electrons/Cooper pairs between the superconducting dots and the metal isn’t high. Low transmission is caused by a physical barrier, or by a difference of the fermi velocities between the two materials.

In this work we have just scratched the surface on the influence of a barrier and low transmission on the bose metal state, and many aspects of this subject are yet to be covered. Clearly, there is much work to be done in the future to shed further light on this issue.

7. Bibliography

[1] S. Sachdev, C. Buragohain, M. Vojta, Quantum impurity in a nearly critical two-dimensional antiferromagnet, Science, 286 (1999) 2479-2482.

[2] J. Bardeen, L.N. Cooper, J.R. Schrieffer, Theory of superconductivity, Physical review, 108 (1957) 1175.

[3] P.W. Anderson, Theory of dirty superconductors, Journal of Physics and Chemistry of Solids, 11 (1959) 26-30.

[4] R. Crane, N. Armitage, A. Johansson, G. Sambandamurthy, D. Shahar, G. Grüner, Fluctuations, dissipation, and nonuniversal superfluid jumps in two-dimensional superconductors, Physical Review B, 75 (2007) 094506.

[5] D. Shahar, Z. Ovadyahu, Superconductivity near the mobility edge, Physical Review B, 46 (1992) 10917.

[6] B. Sacépé, T. Dubouchet, C. Chapelier, M. Sanquer, M. Ovadia, D. Shahar, M. Feigel'man, L. Ioffe, Localization of preformed Cooper pairs in disordered superconductors, Nature Physics, 7 (2011) 239.

[7] S. Poran, E. Shimshoni, A. Frydman, Disorder-induced superconducting ratchet effect in nanowires, Physical Review B, 84 (2011) 014529.

[8] D. Haviland, Y. Liu, A.M. Goldman, Onset of superconductivity in the two-dimensional limit, Physical Review Letters, 62 (1989) 2180.

[9] N. Marković, C. Christiansen, A. Goldman, Thickness–magnetic field phase diagram at the superconductor-insulator transition in 2D, Physical review letters, 81 (1998) 5217.

[10] B. Sacépé, C. Chapelier, T. Baturina, V. Vinokur, M. Baklanov, M. Sanquer, Disorder-induced inhomogeneities of the superconducting state close to the superconductor-insulator transition, Physical review letters, 101 (2008) 157006.

[11] S. Poran, T. Nguyen-Duc, A. Auerbach, N. Dupuis, A. Frydman, O. Bourgeois, Quantum criticality at the superconductor-insulator transition revealed by specific heat measurements, Nature communications, 8 (2017) 14464.

[12] C. Marrache-Kikuchi, H. Aubin, A. Pourret, K. Behnia, J. Lesueur, L. Bergé, L. Dumoulin, Thickness-tuned superconductor-insulator transitions under magnetic field in a-NbSi, Physical Review B, 78 (2008) 144520.

[13] T.y.I. Baturina, D.R. Islamov, J. Bentner, C. Strunk, M. Baklanov, A. Satta, Superconductivity on the localization threshold and magnetic-field-tuned superconductor-insulator transition in TiN films, Journal of Experimental and Theoretical Physics Letters, 79 (2004) 337-341.

[14] M. Strongin, R. Thompson, O. Kammerer, J. Crow, Destruction of superconductivity in disordered near-monolayer films, Physical Review B, 1 (1970) 1078.

[15] R. Dynes, A. White, J. Graybeal, J. Garno, Breakdown of eliashberg theory for two-dimensional superconductivity in the presence of disorder, Physical review letters, 57 (1986) 2195.

[16] M. Paalanen, A. Hebard, R. Ruel, Low-temperature insulating phases of uniformly disordered two-dimensional superconductors, Physical review letters, 69 (1992) 1604.

[17] A. Yazdani, A. Kapitulnik, Superconducting-insulating transition in two-dimensional a-MoGe thin films, Physical review letters, 74 (1995) 3037.

[18] C. Bøttcher, F. Nichele, M. Kjaergaard, H. Suominen, J. Shabani, C. Palmstrøm, C. Marcus, Superconducting, insulating and anomalous metallic regimes in a gated two-dimensional semiconductor–superconductor array, Nature Physics, 14 (2018) 1138.

[19] Z. Han, A. Allain, H. Arjmandi-Tash, K. Tikhonov, M. Feigel'Man, B. Sacépé, V. Bouchiat, Collapse of superconductivity in a hybrid tin–graphene Josephson junction array, Nature Physics, 10 (2014) 380.

[20] T.I. Baturina, V.M. Vinokur, Superinsulator–superconductor duality in two dimensions, Annals of Physics, 331 (2013) 236-257.

[21] J.M. Martinis, K. Osborne, Superconducting qubits and the physics of Josephson junctions, arXiv preprint cond-mat/0402415, (2004).

[22] J. You, F. Nori, Superconducting circuits and quantum information, arXiv preprint quant-ph/0601121, (2006).

[23] A. Frydman, The superconductor insulator transition in systems of ultrasmall grains, Physica C: Superconductivity, 391 (2003) 189-195.

[24] R.P. Barber Jr, R.E. Glover III, Hyper-resistivity to global-superconductivity transition by annealing in quench-condensed Pb films, Physical Review B, 42 (1990) 6754.

[25] R. Dynes, J. Garno, J. Rowell, Two-dimensional electrical conductivity in quench-condensed metal films, Physical Review Letters, 40 (1978) 479.

[26] D. Sherman, G. Kopnov, D. Shahar, A. Frydman, Measurement of a superconducting energy gap in a homogeneously amorphous insulator, Physical review letters, 108 (2012) 177006.
[27] R.P. Barber Jr, L. Merchant, A. La Porta, R.C. Dynes, Tunneling into granular Pb films in the superconducting and insulating regimes, Physical Review B, 49 (1994) 3409.
[28] Y.S. Li, Signature of Cooper pairs in the non-superconducting phases of amorphous superconducting tantalum films, Superconductor Science and Technology, 28 (2014) 025002.
[29] E. Abrahams, P. Anderson, D. Licciardello, T. Ramakrishnan, Scaling theory of localization: Absence of quantum diffusion in two dimensions, Physical Review Letters, 42 (1979) 673.
[30] S. Issai, Is hopping a science?: selected topics of hopping conductivity, World Scientific, 2015.
[31] C. Christiansen, L. Hernandez, A. Goldman, Evidence of collective charge behavior in the insulating state of ultrathin films of superconducting metals, Physical review letters, 88 (2002) 037004.
[32] P. Phillips, D. Dalidovich, The elusive Bose metal, Science, 302 (2003) 243-247.
[33] I. Tamir, A. Benyamini, E. Telford, F. Gorniaczyk, A. Doron, T. Levinson, D. Wang, F. Gay, B. Sacépé, J. Hone, Sensitivity of the superconducting state in thin films, Science advances, 5 (2019) eaau3826.
[34] S. Eley, S. Gopalakrishnan, P.M. Goldbart, N. Mason, Approaching zero-temperature metallic states in mesoscopic superconductor–normal–superconductor arrays, Nature Physics, 8 (2012) 59.
[35] R. Holm, W. Meissner, Messungen mit Hilfe von flüssigem Helium. XIII, Zeitschrift für Physik, 74 (1932) 715-735.
[36] G. Deutscher, P. de Gennes, In Superconductivity, Vol. 2, Ch. 17, Ed.: Parks, RD New York: Marcel Dekker, (1969) 1005.
[37] O. Bourgeois, A. Frydman, R. Dynes, Inverse proximity effect in a strongly correlated electron system, Physical review letters, 88 (2002) 186403.
[38] P. De Gennes, E. Guyon, SUPERCONDUCTIVITY IN" NORMAL" METALS, Phys. Letters, 3 (1963).
[39] P. de Gennes, Boundary effects in superconductors, Reviews of Modern Physics, 36 (1964) 225.

[40] P. Hilsch, Zum verhalten von supraleitern im kontakt mit normalleitern, Zeitschrift für Physik, 167 (1962) 511-524.
[41] G. Miao, Spintronics Driven by Superconducting Proximity Effect, SUPERCONDUCTORS–NEW DEVELOPMENTS, (2015) 127.
[42] P. Visani, Superconducting proximity effect between silver and niobium, in, ETH Zurich, 1990.
[43] L. Merchant, J. Ostrick, R. Barber Jr, R.C. Dynes, Crossover from phase fluctuation to amplitude-dominated superconductivity: A model system, Physical Review B, 63 (2001) 134508.
[44] A.I. Buzdin, Proximity effects in superconductor-ferromagnet heterostructures, Reviews of modern physics, 77 (2005) 935.
[45] G. Blonder, M. Tinkham, Metallic to tunneling transition in Cu-Nb point contacts, Physical Review B, 27 (1983) 112.
[46] G. Blonder, M. Tinkham, T. Klapwijk, Transition from metallic to tunneling regimes in superconducting microconstrictions: Excess current, charge imbalance, and supercurrent conversion, Physical Review B, 25 (1982) 4515.
[47] B. Pannetier, H. Courtois, Andreev reflection and proximity effect, Journal of low temperature physics, 118 (2000) 599-615.
[48] N.W. Ashcroft, N.D. Mermin, Solid state physics (saunders college, philadelphia, 1976), Appendix N, (2010).
[49] C. Hwang, D.A. Siegel, S.-K. Mo, W. Regan, A. Ismach, Y. Zhang, A. Zettl, A. Lanzara, Fermi velocity engineering in graphene by substrate modification, Scientific reports, 2 (2012) 590.

תקציר

מחקר של מערכות דו מימדיות החל כבר לפני כמה עשורים. מאז Abrahams et al הציגו את תאוריית "scaling theory" של לוקאליזציה, התקבעה ההנחה שמצב מתכתי אינו יכול להתקיים במערכות דו מימדיות ללא אינטראקציות חזקות. עם כל זאת, לאחרונה קיימים דיווחים על מצב מתכתי במגוון של שכבות מוליכות-על דו מימדיות. במחקר זה, חקרנו את תופעת המצב המתכתי בדו מימד ולאפיין אותו. התמקדנו במערכות גרנולאריות מחזוריות, בהן נראו סימנים מובהקים של מצב מתכתי. כמו כן, במערכות אלו המעבר ממבודד לעל מוליך מושפע בעיקר מאנרגיית הצימוד בין הגרעינים.

במטרה לאפיין את המצב המתכתי, בחנו כיצד הוא מושפע ממחסום פיזיקלי בין הגרעינים העל מוליכים. לשם כך, יצרנו שני סוגי דגמים: דגם אחד המכיל שכבת תחמוצת בין הנקודות העל מוליכות, ודגם שני ללא אוקסיד. ביצענו מדידות הולכה בשני הדגמים בטמפרטורות קרות, במקביל לנידוף שכבות מתכת דקות על הנקודות. שכבות המתכת מגבירות את הצימוד בין הנקודות ומשפיעות על מצב המערכת.

הממצא העיקרי של עבודתינו הוא שהדגם ללא האוקסיד בין הנקודות הראה מעבר ישיר ביו מבודד לעל מוליך, בעוד הדגם עם האוקסיד הציג רוויה בהתנגדות, דבר המרמז על מצב מתכתי.

מסקנתנו היא שמצב מתכתי מופיע במערכות דו מימדיות כאשר מעבר האלקטרונים בנקודת הממשק בין הנקודות העל מוליכות לבין המתכת מעליהן אינו גבוה. דבר זה יכול להגרם או על ידי מחסום פיזיקלי, או חוסר התאמה בין מהירויות פרמי של החומר העל מוליך והחומר המתכתי.

עבודה זו נעשתה בהדרכתו של פרופסור אביעד פרידמן מהמחלקה לפיזיקה, אוניברסיטת בר אילן.

אוניברסיטת בר אילן

מצב מתכתי במערכות גרנולאריות מסודרות

אביטל פריד

עבודה זו מוגשת כחלק מהדרישות לשם קבלת תואר מוסמך במחלקה לפיזיקה,
אוניברסיטת בר אילן

רמת גן, ישראל ה׳תש״פ